DEVOTED TO THE STUDY OF EARTH'S MOON
VOL. 25 NO. 1 SPRING 2006

SELENOLOGY

*The Journal of
The American Lunar Society*

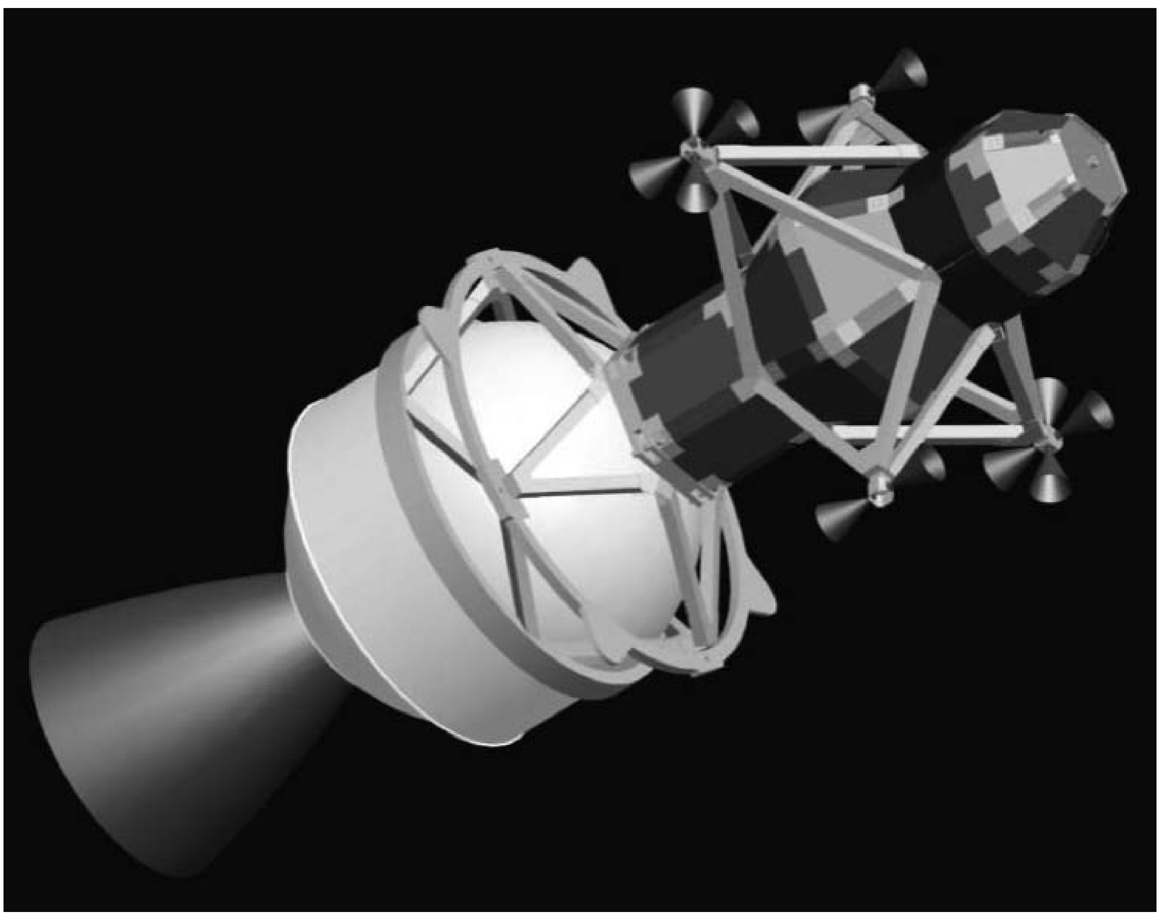

Selenology

Vol. 25 No. 1 - Spring 2006

The official journal of the American Lunar Society, an organization devoted to the observation and discovery of the earth's moon

TABLE OF CONTENTS:

The SMART-1 Impact On the Moon 2

Vertical Studies About Rupes Cauchy 7

Highlights From the 37th Lunar and Planetary Science Conf. 13

Visibility of the Aluminum Line In the SMART-1 Impact 20

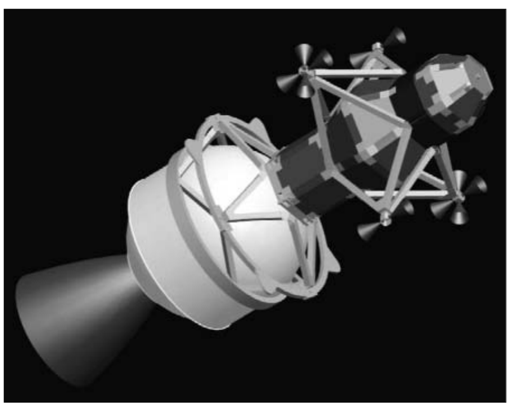

COVER:

Artist's impression of the Brown University Lunar Impactor, FLASH. See page 19.

Selenology, Vol. 25 No. 1, Spring 2006. A publication of the American Lunar Society.
President: Eric Douglass; Vice President: Steve Boint; Editor: Francis G. Graham.

See our website at www.otterdad.dynip.com/als/

Send manuscripts, general observations, and other correspondence to:
Francis G. Graham, Kent State University East Liverpool Campus, 400 E. 4th St., East Liverpool, OH 43920
Phone: 330-382-7466 — E-mail: fgraham@eliv.kent.edu.
Send photographs and drawings that do not accompany a manuscript to:
Steve Boint — E-mail: sboint0362@msn.com
Send changes of address to Eric Douglass at ejdftd@mindspring.com

THE SMART-1 IMPACT ON THE MOON

By Francis G. Graham
US Amateur Observations Coordinator, SMART -1 Impact

[*This article relies upon the impact model and various reports by Bernard Foing of the European Space Agency and colleagues. I have added some ideas of my own, but none in conflict with the models*.]

The SMART-1 impact on the moon might be profitably observed in several ways by amateur astronomers with large instruments.

Time of Impact

At present, the SMART-1 probe is scheduled to impact on the night side of the Earth-facing hemisphere of the moon on the evening of 2-3 September, 2006. The most probable time of impact is 2:00 UT September 3, which is 10 PM, September 2, Eastern Standard Time. At that time, the moon will be at R.A. 18 h 29m 13s, Dec. -28^{o} 27' 32", true equatorial geocentric coordinates, at a distance of 377,338 km. . Thus the moon will be near its most southern point in Sagittarius. For observers in Eastern North America, it will be two hours past its transit of the meridian; the moon will set at 00:21 EDT. The moon will be 72% sunlit, waxing.

It is possible the impact will occur: on the previous orbit, in which case it would be 5 hours before the time stated; or 5 hours after the stated time, on the following orbit. The reason is that the probe is coming into the moon at a very shallow angle of one degree! It could also impact an unknown high topographical high up to 2 hours before expected or 2 hours after, on each possible impact orbit.

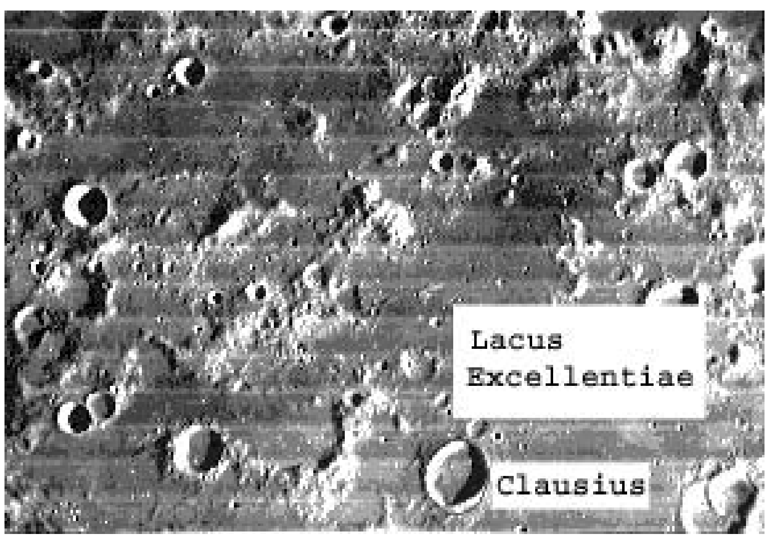

Fig. 1 Impact Site : Lacus Excellentiae

If a planned orbit adjustment scheduled for June 23 to July 8 is not successful, then the probe will impact on August 27. However there is every reason to believe the burn will go as planned, and subsequent adjustments July 26 and August 30 will too, (which will select the orbit of impact even more), to the one which terminates at 2:00 UT September 3.

Visibility on the Earth

At the time of impact, the side of Earth facing the moon will extend from Honolulu to the Canaries, with the moon setting near the Canaries. Observatories in the Western United States will get a twilit view immediately after dusk; observatories in Chile and South America are the most favored, however. The moon will be at zenith over the Pacific approximately halfway between Easter Island and the coast of Peru. Places west of the California/Nevada border will be in sunlight. The observatories in Hawaii will also be in sunlight, with the moon having just risen. If the impact occurs on the following orbit, as may happen, then the western and Hawaiian observatories are favored. If the impact occurs on the orbit previous, then the Eastern United States and the Chilean Observatories will be in sunlight, and the Canaries will be favored.

Location of Impact

At the time of impact, SMART 1 will be orbiting the moon in an orbit with apolune, or farthest point from the moon, at approximately 4420 km.

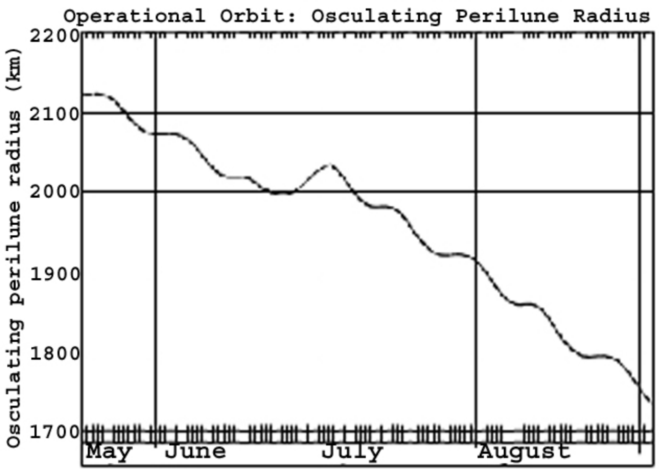

Fig. 2 Decay of the Perilune

and perilune, or closest point, just intersecting or immediately above the lunar surface. The orbit will be inclined 90.6 degrees, which means it will orbit essentially north-south.

The location of the perilune on 2-3 September will be 36S, 44.2 W on the lunar globe, which is in Lacus Excellentiae ("The Excellent Lake"). The probe is expected to impact near the perilune point into a topographically elevated feature. The most probable impact point is 34S, 44.13 W in Lacus Excellentiae north of the crater Clausius. However, if the probe impacts on the previous orbital approach to perilune, which is possible, then the impact will most probably be at 36.5 S, 41.4 W. If it impacts on the following orbital approach to perilune the impact will be most probably at 37S$\pm 2^{o}$, 47 W. Figure 1 is a Lunar Orbiter 4 picture of Lacus Excellentiae; figure 4 shows the topographic features, derived from Clementine probe data, near the final impact point, the elevation topographical lines showing elevations in order of 1 meter. The straight, nearly vertical lines are the SMART 1 orbits, the line in the middle shows the most probable impact orbit and the dot: the perilune. The lines on the right of the center line represent the previous two orbits, the lines on the left the following two orbits. Immediately north of the perilune on the center line is an elevated ridge. It is this ridge the SMART-1 probe is predicted to strike, as it travels from north to south on its orbit. The ridge itself rises in a 2-8 degree slope, the probe will come to it about 1 degree downward and southward from the horizontal.

The lack of highly detailed information on the lunar topography 400 km north or south of Lacus Excellentiae makes an exact prediction of impact impossible; we can only give the most probable. It is possible the probe might just barely clear the ridge on the center orbit and impact on the following orbit.

Orienting the SMART-1 solar panels vertically with respect to the lunar surface may assure impact at the desired location, rather than miss the topographical feature by a few meters and go on to the next orbit. The efficacy of this would depend on how much torque the impacting panels can give the remainder of the spacecraft, and the scale of the uncertainties of the closest approach to the topographical feature. If the scale is thousands of meters of uncertainty rather than scores of meters, the solar panel orientation would, of course, not matter.

Visible Circumstances of Impact

The impact of the SMART-1 probe will be a low velocity (2km/sec = 4,400 MPH) crash, spread out over a large linear swath. The impact energy of the 285 kg craft will thus be about 600 megajoules. If half of this kinetic energy goes into the explosion, the impact will produce a 7.4 magnitude flash. But the impact velocity is lower, so it is likely the percentage of kinetic energy being transformed into heat will be far less, on the order

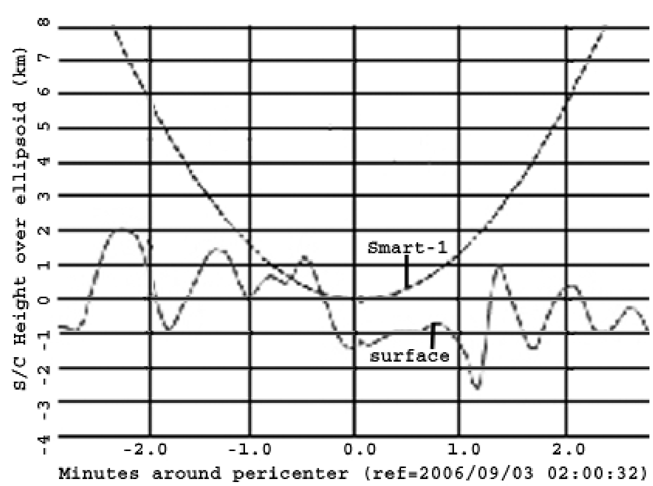

Fig, 3 Perilune Meets Surface

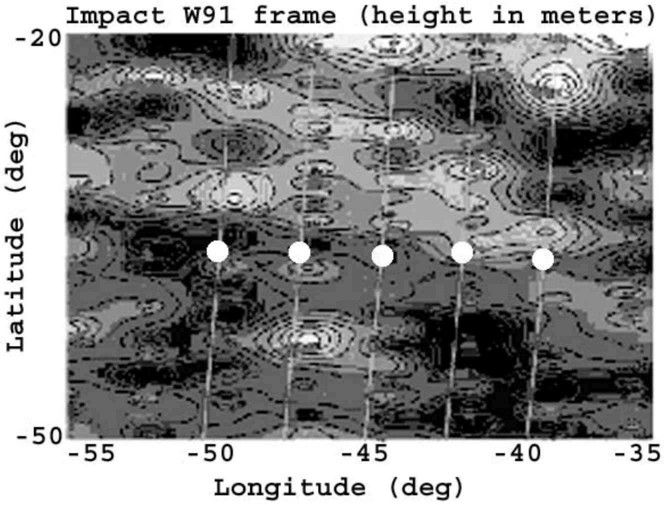

Fig. 4 Impact Map of Final Orbits

of 1% to 0.1% The flash may then be magnitude 16. The duration of the impact flash will be 20 milliseconds.

The flash will also be caused by 3 kilograms of fuel ullage, mainly hydrazine, N_2H_4 (which may raise a significant portion of the 200 kg of aluminum above the 600 Celsius point but not to vaporization).

The impact will likely make a crater 5- 10 m in size, shaped like Schiller (elongated). 10-80 cubic meters of excavation will occur, of which 80% will be an unheated, cold ejecta plume. The dominant ejecta size with be about 15 microns per dust grain. The area of the ejecta could be as high as 25 square kilometers, which would produce a fuzzy appearance for telescopes that can image reflected Earthshine. This would require a telescope of 2 meters aperture or larger.

The dust will be ejected with a wide distribution of velocities, the most probable normal (vertical) component will be 130 m/s. However, a small fraction will be greater than 280 m/s. These particles have enough velocity to ascend upward into the sunlight and be visible. The best modeling gives the magnitude of the plume as:

$$V = 11.5 - 2.5 \log (f/1\%).$$

So if only 1% of the plume exceeds 280 m/s, the magnitude of the sunlit-visible plume would be 11.5. That is, it would appear as a magnitude 11.5 centrally condensed “comet” above the night surface of the moon.

This is what one can hope to see of the SMART-1 impact.

Spectroscopy

Observers with spectroscopes can hope to see evidence of the artificial nature of the impact. Aluminum vapor lines will be absent due to the low velocity of the impact, but other spectroscopic features should be visible.

The reaction

$$N_2H_4 \rightarrow NH_3 + H + N$$

will be facilitated by the thermal energy of impact and produce excited monatomic hydrogen. Thus, Balmer lines of emission will be visible in the spectrum of the flash and the Paschen and Brackett lines in the near-infrared. Again, a large aperture will be required since the total magnitude of the impact can't be brighter than 7.4. In addition, the craft contains about 260 grams of xenon gas which may produce visible lines (such as the 5419 Angstrom line). There are also 14 meters of carbon fiber arrays in the solar panels, but it is uncertain what effect they will have.

The spectroscopy slit should be oriented north-south along the final impact trajectory.

Practice Sessions

The moon will have the same phase as the Impact Day on the evening of July 6-7, and on August 3-4 or 4-5, and so practice sessions can be developed on those days. Astronomers must remember that these observations are a one-shot deal; not since 300 kg Hiten hit the moon at 2.7 km/sec. with 1 kg of hydrazine has there been a similar event. No events like this are scheduled further. The wise observer will prepare several possible observation sites, using cloud cover predictions to finally select between them. Large aperture, portable telescopes are favored.

Observations of the Spacecraft

The spacecraft itself will be magnitude 19 and will be in the sunlight up to 4 minutes before impact. Observing the final orbit of the spacecraft and the time it becomes no longer visible will be invaluable for understanding the final impact. If the solar panels are aligned vertically, the spacecraft will be dimmer. In any case, a 3-meter or larger telescope is required to see the magnitude 19 spacecraft.

Visual Observations

Telescopes for visual observation should be at least 1 meter in diameter, comfortably more, and have a field of view of about 1 arc-minute centered on the impact area.

Infrared Imaging

In the infrared the flash should persist longer, but a large telescope is required. 0.5 arc-second resolution is needed, so adaptive optics must be used. Very large professional telescopes will be used for infrared imaging.

Expect the Unexpected

The flash may also reveal some things about the lunar area upon which it occurs. We have every reason to expect that the low-volatiles of the lunar soil are going to produce no significant emission. But there are many possibilities, each with low probability in impact situations. One recalls the surprises that the impact on Jupiter of Shoemaker-Levy 9 in 1994 produced. Even the Hiten impact produced at least one surprise: a flash signature on the K-band due to Br gamma emission.

There are few scientific paradigms for dealing with the unexpected, but there is a philosophical guide. The Great Chain of Being in the 18th century influenced the encyclopedists; it states that since the Universe is so large, anything that is possible actually exists somewhere (the principle of plenitude). This philosophical principle also asserts that the Universe is continuous, that is, every phenomenon shares with other phenomena some attributes. Finally, this philosophical principle suggests these phenomena have gradation, in some hierarchical order based on magnitude of some attribute.

How does this principle reflect on the unexpected? If many things are possible at a given time and place, though each has a very low probability, one is bound to happen; this is an inversion of the principle of plenitude. It is not always possible for modelers to list exhaustively all the possible events of vanishingly low probability although Fritz Zwicky's morphological method (See Morphological Methods in Astronomy, by F. Zwicky) might serve as a guide to listing them exhaustively. The difficulty is: to have instruments and experiments designed for each of the low probability events, one would have to array extraordinary time and resources. The best chance is to have the widest bandwidth and lowest signal-

Table 1: Mineralogy Sites

Tycho	LC10	-43.40	348.90	East	Large crater; gabbroic plutons
Alphonsus	ALP1	-13.70	356.00		DMD, dark halo crater
Apollo 16	AP16	-9.00	15.50		Landing site, calibration check
Apollo 14	AP14	-3.70	342.50		Landing site, calibration check
Luna 16	LC34	-0.40	56.18		Landing site
Apollo 11	PC4	0.67	23.47		Landing site
Reiner Gamma	REI4	4.95	298.70		Swirl
Luna 24	LU24	12.50	62.25		Landing site, calibration check
Apollo 17	PC9	20.19	30.77		Landing site
Aristarchus	ARI2	23.23	313.47		Aristrachus crater, crustal mat.
Apollo 15	AP15	26.10	356.30		Landing site, calibration check
Gruithuisen	Delta 1	35.90	320.45		Delta dome, early volcanism

to-noise. The two are not always simultaneously possible.

Post Impact Observations

It would be useful to see the area in sunlight after the impact. This will occur two Earth days later. As the Sun rises higher and higher over Lacus Excellentiae, observers can see the ejecta blanket and note how its photometric properties change from an impact of an object of this type. It would also be interesting to see if any of the artificial elements of the spacecraft (e.g., the carbon fibers—carbon is rare on the moon; there is less carbon on the lunar surface that would be expected from the impact of carbonaceous chondrites) affect the photometric properties. The first period of post-impact sunlit observations extends from late September 4 to September 17. The actual impact crater itself, 5- 10 meters in diameter, will be much too small to image from Earth and must await the next lunar reconnaissance mission.

The mineralogy of the area can be examined pre-and post-impact. Dr. Foing has prepared a table of areas of the moon for which mineralogical characteristics can be compared using wide-band reflectance spectroscopy.

Finally, please let me know of your plans and your results. My contact address is:

Francis Graham, Dept. Physics
Kent State University
Kent, OH 44240
fgraham@kent.edu 330-382-74661

Be Published In Selenology!

DO YOU DRAW images of lunar features you observe? Is your new digital camera providing amazing images of craters, mountains or maria? Have you mastered the difficulties of coupling your 35mm to the telescope? Submit your images to *Selenology*. While interesting articles are the main feature of the journal, it's the pictures provided by your participation that produce the warmth of each issue. You know the excitement of viewing the work of others, help keep that excitement going by sharing your images with all of us**!**

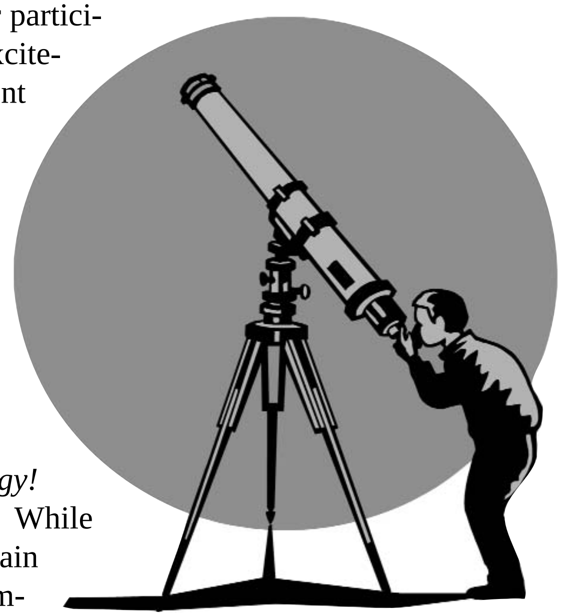

PERHAPS YOU HAVE EXAMINED the Clementine maps for the mineralogy and perused the scholarly literature for more clues about your favorite lunar feature? Share your information with *Selenology's* readers! Or maybe you have multiple photos or drawings of the feature as the shadows alternately reveal and hide its different facets.

LET YOUR WORK GRACE THE PAGES of *Selenology!* Give your fellow readers the opportunity to wonder! While *Selenology* can't publish every submission it receives, we remain eager to publish the work of the American Lunar Society's members—**THIS IS YOUR JOURNAL!**

Send article submissions to: fgraham@eliv.kent.edu.
Send drawings and photographs not part of an article to: sboint0362@msn.com

VERTICAL STUDIES ABOUT RUPES CAUCHY

By Christian Wöhler, Raffaello Lena, Maria Teresa Bregante, Paolo Lazzarotti, Jim Phillips
GLR group

Introduction

The lunar tectonic fault Rupes Cauchy is situated in the eastern part of Mare Tranquillitatis. Mare Tranquillitatis lies on the site of an ancient and large basin, irregular in outline, formed by a major impact during pre-Nectarian time. This basin has been flooded by basaltic lavas whose ages range from 3.8 to 3.3 billion years and are mapped as Upper Imbrian by Wilhelms (1987). Composition and stratigraphy of the basaltic lavas in Mare Tranquillitatis have been extensively studied (Staid et al. 1996; Rajmon and Spudis 2001). In the region around the 12 km crater Cauchy in north-eastern Mare Tranquillitatis, the well-known tectonic features Rima Cauchy (a graben) and Rupes Cauchy (a fault) are situated.

Several domes are apparent along the extension of Rupes and Rima Cauchy, which are in turn oriented radially to the Imbrium basin. Domes associated with a graben along a strike are interpreted to be formed by very shallow dikes (Petrycki et al. 1999). Rima and Rupes Cauchy and the nearby domes are situated within a topographically high region (the eastern part of the Tranquillitatis basin lies higher than its western part) of high-TiO_2 basalts that appears strongly blue in Clementine colour ratio data (Staid et al. 1996).

When Rupes Cauchy is observed near the terminator at sunrise, a shadow can be seen west of the fault. During the lunar day, the width of this shadow decreases. At sunset, the fault appears very bright because the sun shines more steeply on the surface of the fault than on the surrounding mare surface. This observation demonstrates that the mare east of Rupes Cauchy is higher than the mare surface west of it. In this article we illustrate the results of a study about the slope and height of Rupes Cauchy.

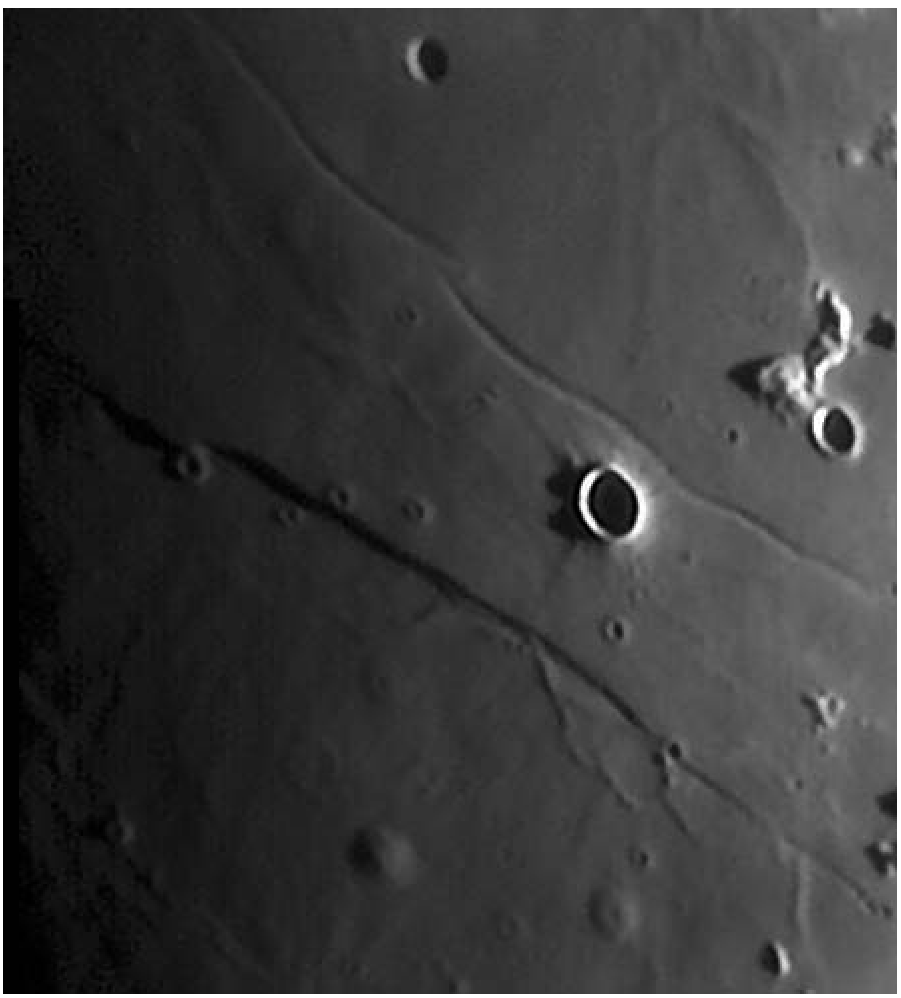

Fig. 1 Rupes Cauchy Under Low Illumination

Instruments and measurements

Figure 1 shows Rupes Cauchy under low solar illumination. This image was taken on April 13, 2005, at 19:24 UT by P. Lazzarotti using a 25 cm Newtonian telescope. The local solar altitude was computed for different locations along the fault with the Lunar Observer's Toolkit software by H. D. Jamieson. The image was rotated such that the shadows are oriented

Fig. 2 Rupes Cauchy : Sunset Illumination

horizontally along the pixel rows in the direction of solar illumination, i.e. in east-west direction (cf. Fig. 4a as an illustration of how to measure the shadow length). Hence, in Fig. 1 north is to the top and west to the left. The coordinates of several locations along the fault were determined by superimposing the image of Fig. 1 onto the corresponding Lunar Aeronautical Chart. The undistorted scale of the image amounts to 365 m per pixel, computed based on the crater Cauchy of 12.4 km diameter. Note that the circular crater is perspectivally distorted into an ellipse in the image. So, the diameter of the crater, measured in km, is divided by the major axis of this ellipse, measured in pixels, to obtain the undistorted image scale. Now a shadow length *L* measured in pixels can be expressed in km. The measured shadow lengths were corrected for foreshortening with the factor $1/\cos \lambda_{eff}$, where λ_{eff} represents the effective selenographic longitude relative to the observed centre of the apparent (due to the effect of libration) lunar disk. The centre of the lunar disk has the selenographic coordinates (λ_c, β_c), which can be obtained from an ephemeris. It can be shown by applying spherical trigonometry that the effective coordinates (λ_{eff}, β_{eff}) relative to the apparent disk centre are given by:

$$\beta_{eff} = \arcsin [\cos\beta_c \sin\beta - \sin\beta_c \sin\lambda_c \sin\lambda \cos\beta - \sin\beta \cos\lambda_c \cos\lambda \cos\beta] \tag{1}$$

$$\lambda_{eff} = \arcsin [(\cos\lambda_c \sin\lambda \cos - \sin\lambda_c \cos\lambda \cos\beta) / \cos\beta_{eff}] \tag{2}$$

where the selenographic longitude and latitude are given by λ and β, respectively. The results of our shadow length measurements are shown in Table 1. Note that if no high accuracy is required, libration may be neglected and λ_{eff} approximated by λ when compensating for foreshortening. The height difference *h* corresponding to a measured shadow length *L* is given by:

$$h = L \tan \alpha \tag{3}$$

where α denotes the local solar altitude.

Fig. 2 displays Rupes Cauchy under sunset illumination. This image was taken on September 03, 2004, at 04:05 UT by P. Lazzarotti, using the same equipment as for Fig.1. In this image, the fault appears as a bright line. The undistorted scale of the image amounts to 353 m per pixel. The width of the fault, measured perpendicular to the direc-

Table 1: Shadow length measurements obtained using the image shown in Fig. 1.

Longitude [°]	Latitude [°]	Solar altitude [°]	shadow length [pixels]	Shadow length (corrected for foreshortening) [pixel]	shadow length [km]	Height [m]
35.50	10.08	1.32	15±1	18.42	6.72±0.36	142±10
35.66	10.00	1.48	18±1	22.15	8.08±0.36	190±10
36.33	9.66	2.15	17±1	21.10	7.70±0.36	271±10
36.66	9.49	2.47	17±1	21.19	7.73±0.36	316±10
37.16	9.33	2.97	15±1	18.82	6.87±0.36	342±20
38.33	8.50	4.13	9±1	11.47	4.18±0.36	296±20
38.50	8.33	4.30	8±1	10.22	3.73±0.36	276±20

tion in which it is running, was determined by measuring the pixel coordinates (u_1, v_1) and (u_2, v_2) of corresponding locations on both sides of the fault, respectively (cf. Fig. 4b). Shadow length and fault width are thus measured in different directions. The upper left corner of the image has the coordinates $u = v = 0$. The image must be oriented north to the top and west to the left. The fault width w in pixels, corrected for foreshortening, is given by:

$$w = \mathrm{sqrt}\left[\left(\left((u_2 - u_1) + |v_2 - v_1| \tan(\beta_{eff} \sin\lambda_{eff})\right) / \cos\lambda_{eff}\right)^2 + \left((v_2 - v_1) / \cos \beta_{eff}\right)^2\right] \quad (4).$$

This rather complex relationship results from the fact that, in the image, distances in the east-west direction are distorted by a different amount than distances in north-south direction. Note that Eq. (4) only holds if location 2 is north of location 1, which also means that $v_2 < v_1$. Eq. (4) corresponds to measuring the width w on a map in simple cylindrical projection (Greeley and Batson, 1990) and is therefore only accurate for low to moderate latitudes and as long as a small latitude range is covered by the width of the fault. Clearly, these conditions are met in our example. The value of w measured in pixels according to Eq. (4) can immediately be translated into kilometres by multiplying it with the previously determined undistorted pixel scale. Our results for the width of Rupes Cauchy are reported in Table 2.

Fig. 3 shows a further image of Rupes Cauchy, taken under strongly oblique sunset illumination. This image was made on October 03, 2004, at

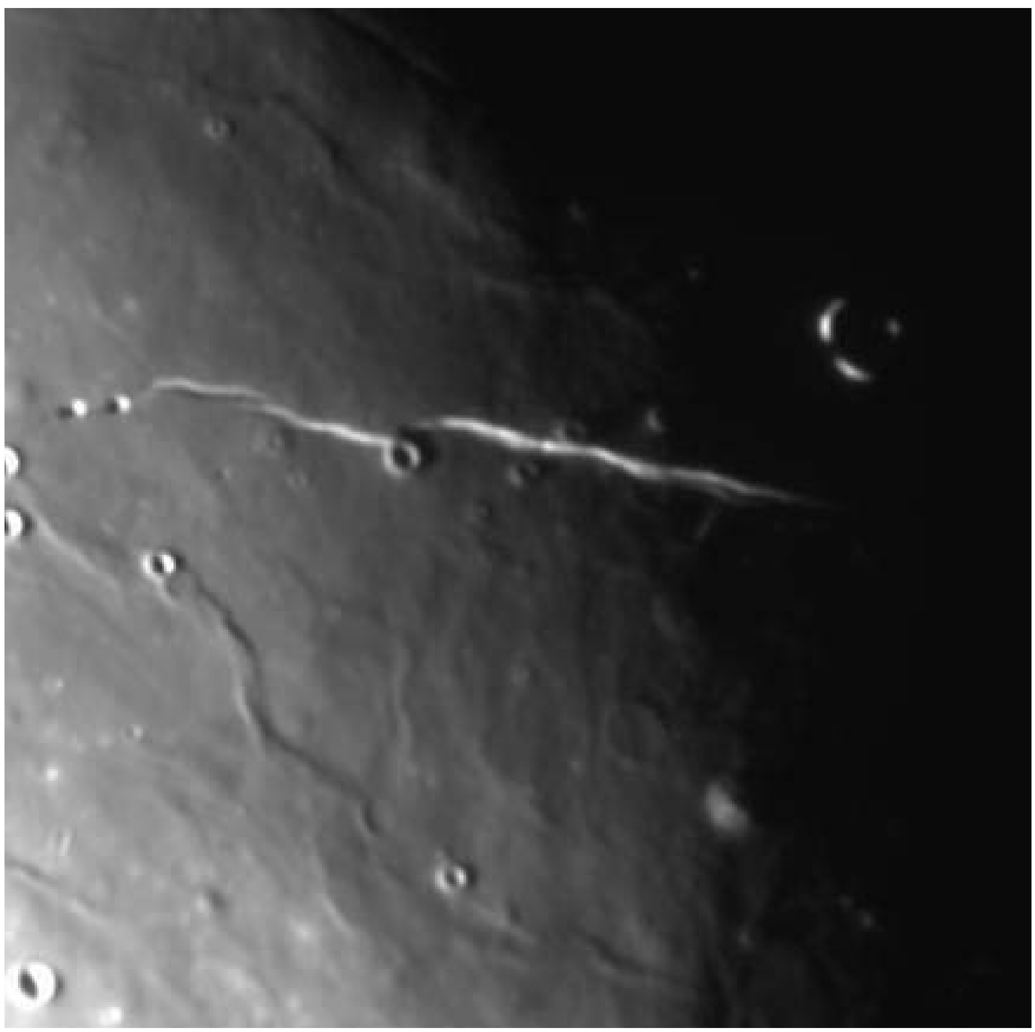

Fig. 3 Rupes Cauchy: Oblique Sunset

Table 2: Measurements of the width of Rupes Cauchy obtained using the image shown in Fig. 2.

Longitude [°]	Latitude [°]	Solar altitude [°]	Width of the fault (corrected for foreshortening) [pixels]	Width of the fault [km]
35.50	10.08	9.64	4.6±1.0	1.6±0.4
35.66	10.00	9.48	4.6±1.0	1.6±0.4
36.33	9.66	8.83	4.6±1.0	1.6±0.4
36.66	9.49	8.50	4.6±1.0	1.6±0.4
37.16	9.33	8.01	4.6±1.0	1.6±0.4
38.33	8.50	6.88	4.6±1.0	1.6±0.4
38.50	8.33	6.68	4.6±1.0	1.6±0.4

07:45 UT by J. Phillips, using a 200 mm TMB refractor. The fault is close to the terminator and appears as a bright line. The undistorted scale of the image was determined to be 460 m per pixel. Measurements of the fault width carried out in this image are reported in Table 3, demonstrating that they are in good agreement with the data obtained for Fig. 2. Based on the data of Tables 1 and 2, the slope ζ of the Cauchy fault was computed using the relation:

$$\zeta = \arctan (h/w) \qquad (5),$$

where h and w denote the height and the width of the fault, respectively, determined for a specific location. The results are reported in Table 4.

Digital elevation map of Rupes Cauchy

Based on the images shown in Figs. 1 and 2, we have generated a digital elevation map (DEM) of a section of Rupes Cauchy, making use of the image-based method for 3D surface reconstruction introduced by Wöhler and Hafezi (2005). Relying on the analysis of at least two pixel-synchronous greyscale images of the scene acquired under very different illumination conditions, this framework combines a shadow analysis of the first image of the surface (allowing for a determination of large-scale altitude differences on the surface at high accuracy) with a variational shape from shading scheme (Horn 1989; Lena et al. 2005) applied to the second image. The shape-from-shading method assumes that, for a given illumination angle and camera direction, the relation between the orientation of a surface element and the amount of light scattered by it into

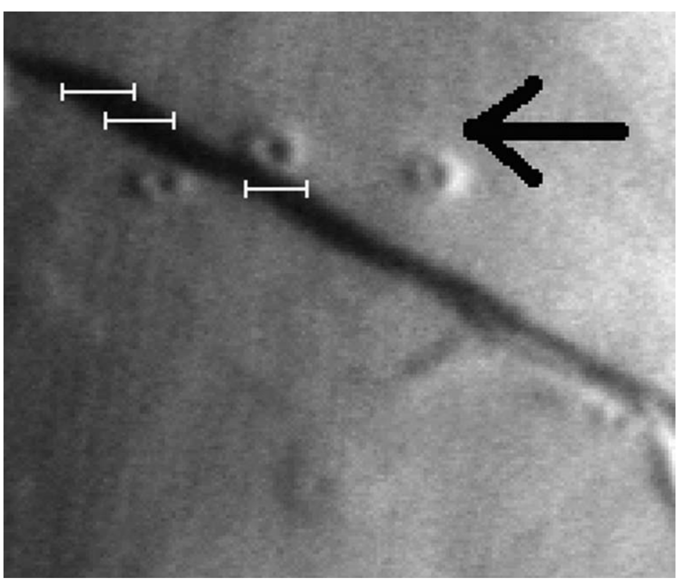

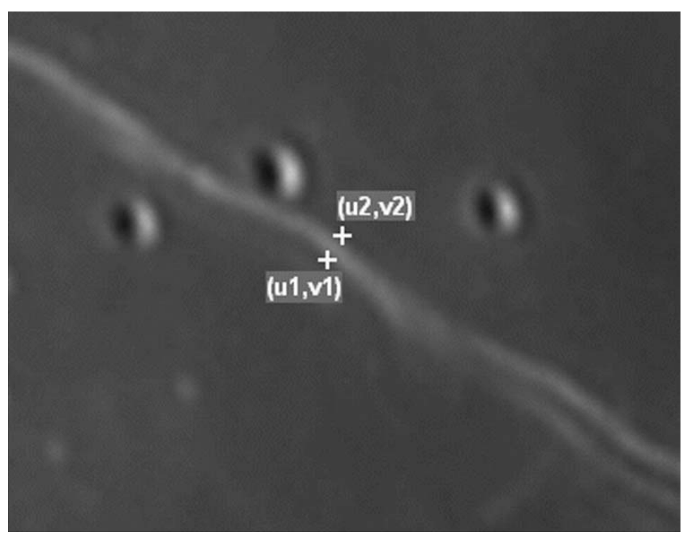

Fig. 4: (a) Illustration of the measurement of shadow length. The large arrow denotes the direction of illumination. (b) Illustration of the measurement of the fault width. In both images, north is to the top and west to the left. For further explanations cf. pp 8-9.

Table 3: Measurements of the width of Rupes Cauchy obtained using the image shown in Fig. 3.

Longitude [°]	Latitude [°]	Solar altitude [°]	Width of the fault (corrected for foreshortening) [pixels]	Width of the fault [km]
35.50	10.08	1.79	3.4±1.0	1.6±0.5
35.66	10.00	1.64	3.5±1.0	1.6±0.5
36.33	9.66	0.97	3.5±1.0	1.6±0.5
36.66	9.49	0.65	4.6±1.0	2.1±0.5

Table 4: Height and slope values obtained for different locations along Rupes Cauchy.

Longitude [°]	Latitude [°]	Width of the fault [km]	Height [m]	Slope [°]
35.50	10.08	1.6±0.4	142±10	5.1±2.2
35.66	10.00	1.6±0.4	190±10	6.8±2.7
36.33	9.66	1.6±0.4	171±10	6.1±2.4
36.66	9.49	1.6±0.4	316±20	11.2±4.4
37.16	9.33	1.6±0.4	342±20	12.1±4.6
38.33	8.50	1.6±0.4	296±20	10.5±4.2
38.50	8.33	1.6±0.4	276±20	9.8±4.0

the camera is known. The gradients of the reconstructed surface are adapted such that the modelled distribution of light reflected from the surface becomes as similar as possible to the observed image. According to Wöhler and Hafezi (2005), an error term that aims at adjusting the altitude differences extracted from the reconstructed surface profile to those derived from shadow analysis is incorporated into the error function to be minimized by the variational shape-from-shading scheme. The algorithm yields the surface gradients and a DEM for the evaluated surface section (Fig. 5), thus illustrating the variable height of Rupes Cauchy.

Results and discussion

Based on shadow length measurements and of the width of Rupes Cauchy, the height and the slope angle of Rupes Cauchy were calculated for several locations. The height amounts to 340 m in the centre and diminishes slightly towards the south. Towards the north, the height decreases until the fault fades away in the mare plane. The slope angle is about 12° for the highest and steepest part of the fault and diminishes towards the north and the south. Height and slope of Rupes Cauchy are thus comparable to those of the famous tectonic fault Rupes Recta in eastern Mare Nubium. For its northern part, a digital elevation map has been generated by Wöhler and Hafezi (2005). Their data reveal that the northern part of Rupes Recta has a height of up to 500 m and a slope of 8.7°.

Future observing schedules of the GLR group are being planned to investigate different lunar rupes on a case by case basis. The collected data and measurements will yield a core set of observations upon which more statistical analysis can be performed.

References

[1] Greeley, R., Batson, R. M. (1990), Planetary Mapping, Cambridge University Press, Cambridge.

[2] Horn, B. K. P. (1989), Height and Gradient from Shading, MIT technical report 1105A.
http://people.csail.mit.edu/people/bkph/AIM/AIM-1105A-TEX.pdf

[3] R. Lena, C. Fattinnanzi, J. Phillips, C. Wöhler. “A study about a dome near Yerkes: observations, measurements and classification”. Selenology, vol. 25, no. 2, pp. 4-10, 2005.

[4] Petrycki, J. A., Wilson, L. (1999), “Volcanic Features and Age Relationships

Associated with Lunar Graben”, Proceedings of the 30th Lunar and Planetary Science Conference, paper #1335.

[5] Staid, M. I., Pieters, C. M., Head, J. W. (1996), “Mare Tranquillitatis: Basalt emplacement history and relation to lunar samples”, Journal of Geophysical Research, vol. 101, no. E10, pp. 213-227.

[6] Wöhler, C., Hafezi, K. (2005), “A general framework for three-dimensional surface reconstruction by self-consistent fusion of shading and shadow features”, Pattern Recognition, vol. 38, no. 7, pp. 965-983.

To become a member of ALS

and receive your subscription to *Selenology*, mail a check for $15 (all countries) to:

Eric Douglass
10326 Tarleton Drive
Mechanicsville, VA 23116

Make the check out to Eric Douglass, President ALS, and be sure to include your email and snail mail addresses.

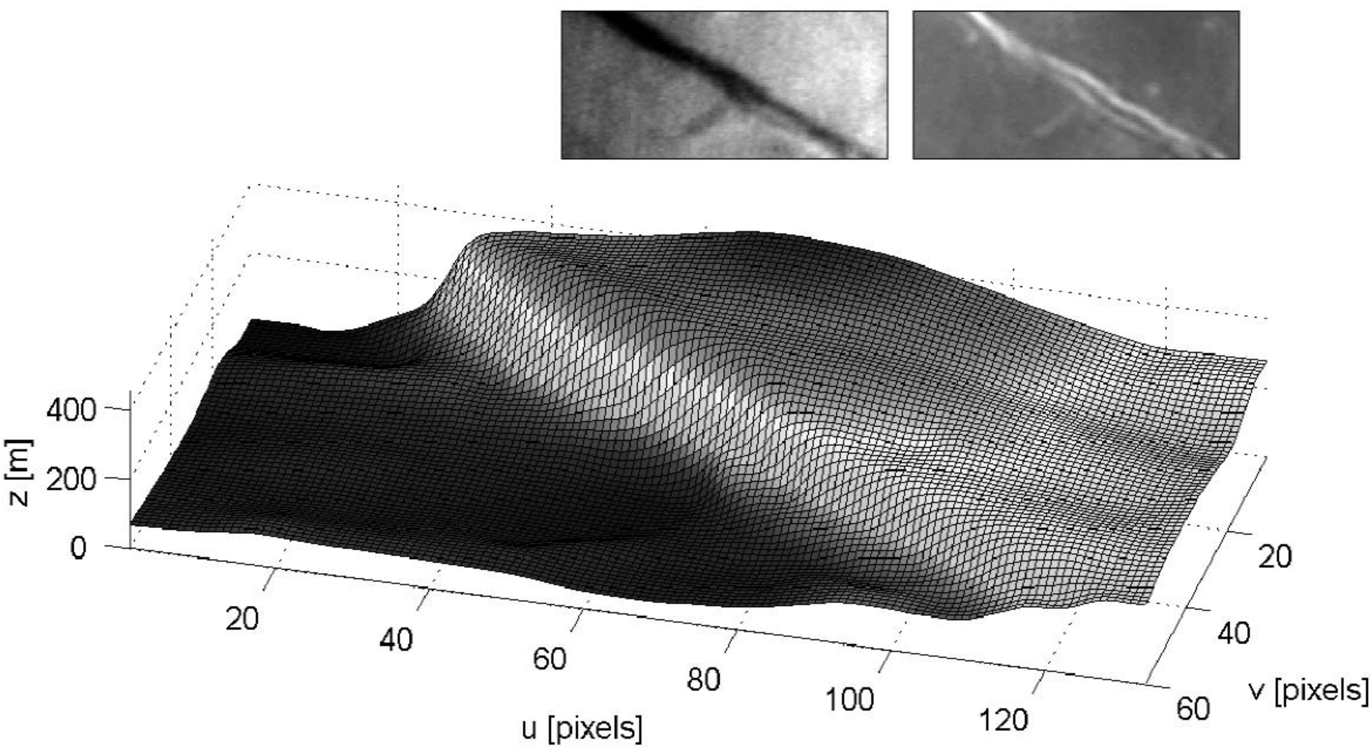

Fig. 5: DEM of a section of Rupes Cauchy. The image regions shown above, from which the DEM was generated, were taken from Figs. 1 and 2, respectively, and were rectified according to simple cylindrical projection.

HIGHLIGHTS OF LUNAR SCIENCE FROM THE THIRTY-SEVENTH LUNAR AND PLANETARY SCIENCE CONFERENCE

By Francis G. Graham
Kent State University

The Thirty-Seventh Lunar and Planetary Science Conference held its yearly meeting in Houston, a tradition that has been uninterrupted since the Apollo 11 Lunar Science Conference was held in 1970. It expanded into other aspects of planetary science beyond the moon in 1979 and then, due to Homeland Security concerns, moved away from the Manned Spacecraft Center into more remote hotel facilities in 2002.

The following are highlights of some lunar science papers that were discussed this year. The information is gleaned from the abstracts of the conference, published as a CD-Rom: Lunar and Planetary Institute Contribution No. 1303.

The abstracts are also available online at http://www.lpi.usra.edu/meetings/lpsc2006/

Analysis of Lunar Orbiter and Apollo Imaging Data

Back in the 1960's and 1970's, it was often said that the treasure-trove of images and samples from Apollo, Lunar Orbiter and the Luna spacecraft would keep scientists busy for decades. Four decades later, this still holds true. Much of the interest comes from new tools for analysis: more sensitive measurements, new kinds of measurements, digitization of the entire data base.

In “Lunar Orbiter Revived-Very High Resolution Views of the moon”, L. Weller et al have presented a digitization of the raw Lunar Orbiter images, available at: http://astrogeology.usgs.gov/Projects/LunarOrbiterDigitization/

M.R. Rosiek et al are using the Lunar Orbiter as well as the Apollo image data set to do topographic mapping. They obtain the elevation from multiple exposures of the same feature, and use a commercial photogrammetric workstation and SOCET SET software from BAE systems.

D.A. Williams and E.J. Grayzeck also are working on archiving of data.

Continued Analysis of Apollo Samples-and Luna Samples

Apollo samples continue to bring a wealth of new information, especially when considered in light of the new information from Lunar Prospector, SMART-1 and Clementine. J.P. Vaughan et al measured the Uranium-Lead ages of lunar apatites. M.A. Wieczorek and S. Huang re-analyzed Apollo 15 and Apollo 17 surface and sub-surface temperature series.

M.M. Abbas et al performed photoelectric emission measurements on Apollo 17 dust grains. These dust grains become electrically charged and are of interest as they may be toxic to humans. In fact, dust smaller than 20 micrometers in size is apparently toxic and Y. Liu et al looked at the magnetic properties of Apollo 17 soil 70051 with the idea of using magnetic fields to separate and mitigate the dust problem in future human settlements on the moon. M.J. Mellin et al also took a look at this unique soil sample, 77051.

T. Arai et al looked again at Apollo 14's oldest mare basalt. The gabbronorite VHK basalts apparently came later. Mare volcanism started about 4.23 billion years ago, but the so-called gabbronorite VHK basalt magmatism continued until 3.8 billion years ago.

J.M. Day et al looked at the rhenium-osmium isotope systematics in mare basalts to examine the accretion, differentiation and late bombardment history of the moon. J. Edmundson et al pointed out problems with the uranium-lead systematics in lunar samples of mare basalt 10017 and norite 78328. T.L. Grove et al re-examined Apollo 15 red glass and found new constraints on melting depth and titanium oxide melt contents of ilmenite saturated residues. J. Levine et al examined implanted and cosmogenic argon 38 and argon 39 in lunar impact spherules (and also the potassium and calcium in them)—an important consideration for models of the lunar atmosphere.

Looking back, J. Longhi and D. Walker looked for the signature of the moon's early magma ocean using the systematics of nickel.

R.T. Pidgeon et al did a modest project examining two lunar zircons. Zircons are very useful because they are rather geochemically isolated and contain trace amounts of lead and uranium which can be dated. It shows how one must be careful in doing analysis and assigning dates. One zircon had another zircon imbedded inside of it. The interior zircon was primary and crystallized 4.31 billion years ago from a melt. Some kind of secondary shock event re-melted the outside, and produced a secondary zircon 4.18 billion years ago. The second zircon, from the Serenitatis region, crystallized 4.281 billion years ago, but underwent a chemical reaction on its rim 4.106 billion years ago. Finally, the zircon ended up in a host breccia from Serenitatis 3.8 billion years ago.

Astronauts Scott and Irwin join geologists in looking at Apollo 15 samples. NASA Photo ID: S71-43203

For Luna 24 samples, L. L. Kashkarov et al looked at chemical modification of Luna 24 grains under solar cosmic ray irradiation.

M.D. Norman and V.C. Bennett inferred impactor populations and lunar crustal compositions from highly siderophile elements in Apollo 16 and 17 melt breccias. And lastly, D.W. Schare examined the origin of Apollo 15 olivine and quartz.

S.E. Braden and M. S. Robinson did an interesting project, photographing thin sections of lunar rocks through GBR filters in a precise photometrically calibrated manner and using the photographs of these thin sections to investigate lunar mineralogy. They were able to correctly derive titanium dioxide abundances.

Clementine, Lunar Prospector and Lunar Polar Ices

Both Clementine and Lunar Prospector produced valuable elemental composition surveys and lunar polar ice searches. Recall the Lunar Prospector data were positive for hydrogen in the lunar polar areas as was the radar reflection from the Clementine probe in the south polar area. The moon, of course, has only a slight axial tilt allowing perpetually shadowed craters near the lunar north and south pole. Since the moon has no atmosphere, once ice arrived in these craters, it could remain for a long time. Interest in determining whether there really are such ices will have a major impact on how a manned lunar mission might be planned.

Lunar Prospector was able to use its gamma ray spectrometer for elemental compositional studies elsewhere on the moon. Some papers at the

Basin	Diameter (km)	Age (gigayears)	Volcanism (gigayr)
Procellarum	3200	4.3	1.2 -3.93
Imbrium	1160	3.92	2.01-3.57
Crisium	1060	3.98	2.3 -3.35
Serenitatis	740	3.98	2.44-3.81
Tranquillitatis	775	4.1-4.2	3.39-3.80

Table 1: Lunar geological sequences

Conference addressed this.

Looking at titanium, iron, calcium, and magnesium as mapped by the Lunar Prospector and using the principle of superposition, H. Yamamoto derived the sequence in Table 1.

A.A. Berezhnoy at the Sternberg Astronomical Institute worked on the correction of Lunar Prospector elemental maps based on errors in the global mapping analysis of thorium and iron gamma ray emission.

J.T. Cahill et al from the University of Hawaii looked at the mineralogy and geochemistry of lunar highlands spectral types; with P. G. Lucey he

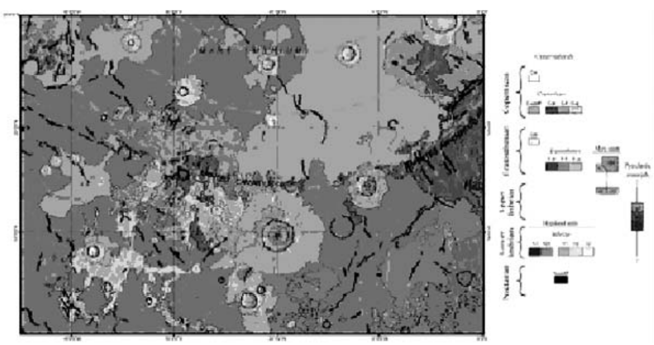

Map of the Copernicus Quadrangle of the moon from the New USGS Maps

looked at magnesian rock types in the lunar highlands. L.R. Gaddis et al is re-doing the entire collection of USGS lunar maps with updated Lunar Prospector data. V.G. Kaydash et al used lunar photometry from the Clementine probe to estimate the Hapke parameters so that the SMART-1 data could be correctly analyzed. D.J. Lawrence worked on improved modeling of the Lunar Prospector neutron spectrometer and its implications for ice at the lunar poles.

There were also radar observations of the lunar poles from Earth. D.B. Campbell et al used the Arecibo radio telescope as a transmitter and the Green Bank Telescope as a receiver in April, 2005, at a wavelength of 13 centimeters. Said Campbell: “These new data support the hypothesis that the south polar hydrogen enhancement measured by [Lunar Prospector] reflects a widely disseminated component of the lunar regolith, rather than any localized concentration of water ice.”

B.A. Campbell et al also used 20-meter resolution radar studies of the Aristarchus plateau and the Gamma Reiner formation, at 13 cm wavelength and 70 cm. wavelength. S. Chevrel at al followed that up with visual photometry and an estimation of the Hapke parameters at the same feature.

Robert Anderson et al suggested using impedance as a way of detecting water ice in martian and lunar regoliths, but this requires a lander with electrodes.

In “Water Delivered to the moon by Comet Impacts”, L. Ong and colleagues used the latest data from Tempel 1 to estimate the water comets give to the polar craters. A comet with a mass of water ice exceeding an exogram (a quadrillion grams) strikes the moon approximately every million years. Norbert Schorghofer and G. Jeffry Taylor showed that most ice would have escaped destruction (from reflected sunlight, cosmic rays, and so forth) over the last billion years and is subsurface at the lunar polar cold traps. It's a very positive note.

Lunar Meteorites

A growing number of lunar samples are obtained as meteorites. As R.L. Korotev stated in his paper, “New Geochemical Data for some Poorly Characterized Lunar Meteorites”: “Lunar meteorites are far more compositionally diverse than meteorites from any other parent body. Several are dissimilar to any Apollo samples.” He showed the similarity, but disproved the pairing of meteorite NWA 2200 with farside sample NWA 482, and looked at Dhofar 280 and 910, and Dar el Gani 916.

R.A. Zeigler analyzed lunar basaltic meteorite NWA 3160. T. Arai used NWA 773 and LAP 02205 to characterize the visible and near infrared spectra of brecciated mare basalts.

T.E. Bunch et al investigated lunar mare basalt gabbro breccias NWA 2700, NWA 2727, NWA 2977 and paired them to NWA 773. Most of these meteorites were found by Mike Farmer.

V.A. Fernandes and R. Burgess did argon-argon studies of the mare basalt meteorites LAP 02205 and EET 96008. There are now over 50 lunar meteorites. Discounting pairings, 37 different samples are known. Only 5 are lunar mare basalts. EET 96008 has an age of 3.22 billion years, LAP 02205, very similar if not identical to NWA 773, has an age of 2.92 billion years. The source regions are thought to be Mare Crisium (due to low titanium content) and northwest Oceanus Procellarum for LAP 02205. They both show an argon disturbance 630 million years ago.

J. Haloda et al introduced new lunar meteorite NEA 003-A, a new lunar mare basalt breccia.

A.J. Irving et al analyzed NWA 3163, a unique meteorite from the deep lunar crust, a mafic granulitic impactite. It was interesting to compare this to B.L. Jolliff's “What is the Composition of the moon's Lower Crust?” which postulated ferroan anorthosites and anorthositic gabbros.

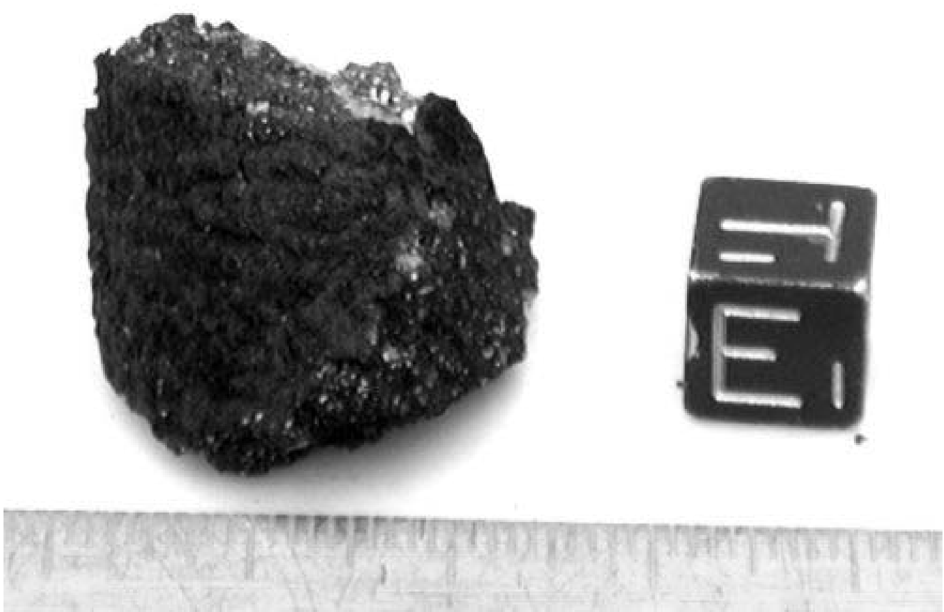

Meteorite 01210 from
http://epsc.wustl.edu/admin/resources/meteorites/met01210.html

K.H. Joy and colleagues examined lunar regolith breccias MET 01210, PCA 02007, and Dar-el-Gani 400, and showed their importance to the SMART-1 mission analysis.

Y. Karouji and colleagues looked at Yamato 983885, another KREEP-rich lunar regolith breccia. E. Koizumi et al. presented “Crystallization of the Lunar Basaltic Meteorites NWA 032 and 479: Preservation of the Parent Melt Composition and Relationship to LAP 02205”.

R.L. Korotev also presented “Geochemistry of a Unique Lunar Meteorite from Oman, a Crystalline Impact Melt Breccia Dominated by Magnesian Anorthosite”. He paired 15 meteoritic stones from Dhofar.

It's important also to learn how lunar meteorites are altered and weathered in Earth's environment while they wait to be picked up and studied. These effects must be considered in reconstructing the meteorite's environment on the moon. K. Nishiizumi, with his colleagues, examined the exposure and terrestrial histories of lunar meteorites LAP 02205, 02224, 02226, 02436, MET 01210 and PCA 02007.

Not only were meteorites from the moon on Earth examined, but meteors hitting the moon were considered in “A Probable Taurid Impact on the Moon” by W.J. Cooke et al. This meteor, which struck the moon Nov. 7, 2005, was observed at the Marshall Space Flight Center with a 10-inch f/4.7 Newtonian and CCD. At visual magnitude 7.3, it represented the energy of 320 tons of TNT. Assuming a luminous efficiency of 0.2%, this was a kilogram-size mass.

There were two other extremely interesting papers on lunar impacts, if papers can be gauged interesting by the opportunities they create for further research. V.V. Shuvalov and N.A. Artemieva did a careful physical analysis of major lunar impactors and asked what fraction of material would make it to Earth. Their analysis was on present-day (last billion years) lunar conditions. For a major hypervelocity impact, roughly half of the material ejected from the moon would be accreted on Earth within only 10 million years, and most of it within 50 thousand years. If this analysis is correct, it gives a way to precisely (within 50,000 years) correlate terrestrial and lunar geological strata— if lunar material can be identified. Indeed, Ordovician meteorites have been found. The authors give an example of the 83-kilometer diameter crater Tycho, formed by an impact 100 million years ago. It was an oblique impact, 30-45 degrees, from a 6-7 kilometer diameter projectile. It ejected 25-100 cubic kilometers of material to Earth, similar to the amount of ash released by the Yellowstone eruption 625,000 years ago. Assuming a 30% loss in the atmosphere, our planet was covered uniformly with Tycho meteorites 0.1-0.3 kg per square meter. This sort of sample is worth looking for.

B.R. Hawke and colleagues also re-examined the whole matter of crater rays (since we are on the subject of Tycho, one of the more prominent rayed craters). The Copernican/Eratosthenian boundary in the lunar strata is partly based on the idea that rays older than 1.1 billion years do not exist. Copernicus is 800 million years old, and it is near that boundary. However, the rayed crater Lichtenberg is 1.68 billon years old and Aristillus and Autolycus, identified as Copernican because of the presence of weak rays, are 1.3 billion and 2.1 billion years old respectively, suggesting rays can persist. Hawke and colleagues recommend that Aristillus, Autolycus, Taruntius, O'Day, and Eudoxus be reassigned to Eratosthenian age, even though they have rays and are erroneously assigned to Copernican age.

Lunar Reconnaissance Orbiter

SMART-1

A number of papers dealt with the SMART-1 probe presently orbiting the moon. Bernard Foing, the SMART-1 primary investigator, and colleagues presented "ESA's SMART-1 Mission: Lunar Science Results After One Year". Much of this was outlined in last

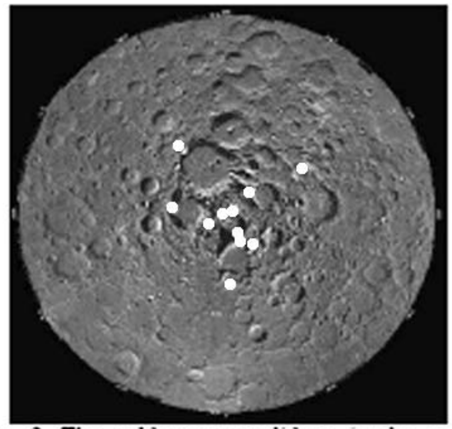

Fig. 2 The cold traps candidates in the northern hemisphere of Moon

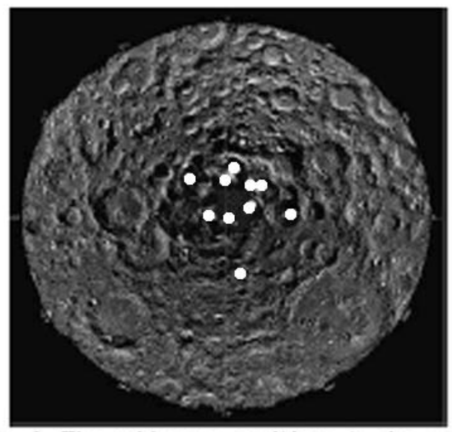

Fig 3 The cold traps candidates in the southern hemisphere of Moon

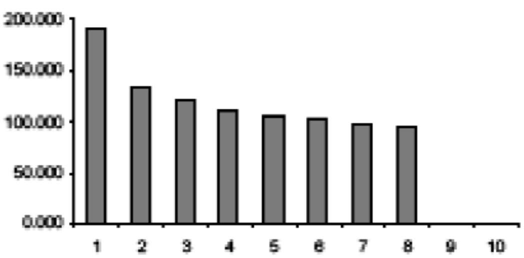

Fig. 4. Collective estimation of Hydrogen content for northern "possible" cold traps candidates

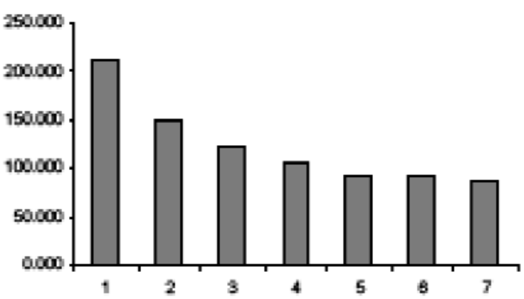

Fig. 5. Collective estimation of Hydrogen content for southern "possible" cold traps candidates

Illustrations from Sanin, et al.

year's Selenology. Jean-Luc Josset also presented “SMART-1 AMIE Camera System”, to familiarize conference attendees with the imaging process used by the probe.

B.J. Kellett and M. Grande presented “X-Ray Fluorescence Observations of the moon: Highlights from the First Year of Observations from D-CIXS on SMART-1”. G.Y. Kramer presented a pair of papers on the subject of searches for high-aluminum mare basalts. P. Cerroni et al. presented “Preliminary Analysis of Colour Information from AMIE on SMART-1” and showed several analytical images, including Mare Ingenii, as examples.

Also, in support of SMART-1 analysis, M.S. Robertson, J.B. Garvin and Bruce Hapke used the Hubble Space Telescope to image the Apollo 17 landing site in the ultraviolet and visible light.

Chandrayaan-1

A number of papers dealt with preparations for lunar probes to be launched. India's first lunar probe, Chandrayaan-1, will be able to settle the lunar water question once and for all. Carle Pieters and colleagues described the Chandrayaan Moon Mineralogy Mapper, or M-cubed, which detects the 2.8 micrometer absorption band of water. It is sensitive enough to detect even trace amounts of water at the lunar poles in reflected Earthshine.

J.N. Goswami, K. Thagarajan and M. Annadurai gave the definitive overview of Chandrayaan, including its M-cubed hyperspectral imager. It also will have a laser altimeter, a terrain-mapping camera, low and high energy X-ray spectrometers and a miniature synthetic aperture radar. It will map the surface concentrations of not only water, but magnesium, aluminum, silicon, calcium, titanium and iron.

Lunar Reconnaissance Orbiter

This NASA probe is also scheduled for launch in the near future and G. Chin and colleagues presented an overview of its instrumentation and expectations. It has a laser altimeter, an orbital camera, a neutron detector to search for water ice (similar to that on Lunar Prospector) , a lunar radiometer to map the entire surface's temperature and look for ice coldtraps near the poles, it will look for Lyman-Alpha line emission in reflected sunlight from the lunar polar areas as an indicator of hydrogen there (which is an indirect indicator of water) and it will have a miniature radar observation demonstrator. It will also carry plastic human tissue simulants and will look for cosmic ray effects on them.

A.B. Sanin and colleagues detailed exactly how the LRO spectrometer will look for water ice at the poles: seeking hydrogen through using the LEND instrument, the Lunar Exploration Neutron Detector, which can find hydrogen (at a concentration of 100 parts per million or less) buried as deeply as 1 to 2 meters below the surface. It has this advantage over Chandrayaan-1: it can look

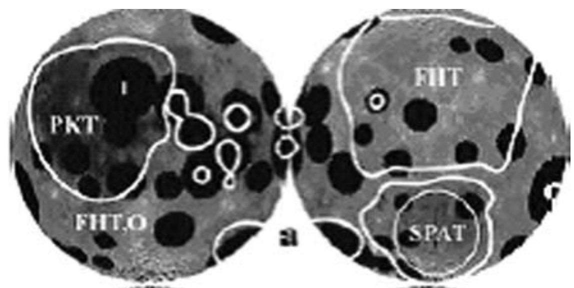

Three Major Terranes of the Moon
PKT=Procellarium KREEP;
FHT=Feldspathic Highland;
SPAT= South Pole Aitken.

deeper. There is the possibility that Chandrayaan, looking nearer to the surface, may see no water, but the LRO may see hydrogen much deeper. This could lead to a public perception that the results are contradictory unless both teams come up with a public statement protocol.

B.T. Greenhagen and D.A. Paige also looked at lunar surface petrology mapping with LRO's Diviner radiometer.

SELENE

The Japanese have a new lunar probe being readied for launch and M. Ohtake and his colleagues delightfully summarized the observational plans. K. Ogawa summarized the development of the X-ray spectrometer. Like Chandrayaan and LRO, there is a quest to find water at the lunar poles. M. Kato and colleagues presented the more definitive overview of this important mission which will have an X-Ray and gamma ray spectrometer, a laser altimeter, radar sounding, and a package called VRAD, which will map the moon's gravitational field better than before; and also two subsats to sample the lunar magnetic field and plasma environment. SELENE is due for launch in August of 2007, will arrive at the moon two months later, and then begin a 100 km circular orbit three weeks after that.

"Why don't they take a dowsing rod?" asked my friend Billy, reminding me that in the USA at least, there is a great need for public education on science and space issues.

In any case, ideas of lunar exploration architecture were presented by B. Boldoghy and colleagues. D.P. Morgan et al proposed a 5 kilogram kamikaze lunar impactor, called FLASH, that would deliberately and cheaply impact the moon with three impactors 500 meters and 1 second apart.

Simply the moon

The new spacecraft and Earth observational data have produced a new view of the moon. Charles Byrne looked at the giant, ancient megabasins and N.E. Petro and Carle Pieters summarized these early impacts as having produced three distinct terranes on the moon. The first, caused by the Oceanus Procellarum megabasin, is a KREEP terrane. The second is the South Pole Aitken basin, another unique terrane with a unique geological history. The third is the feldspathic highland terrane, which covers most of the farside and the southern nearside . Basin ejecta dot the third terrane, ten times more so on the nearside.

J.H. Jones took it one abstraction further, with "Do's and Don'ts on How to Build a Planet, Using the Moon as an Example". He pointed out that the composition of these terranes and the moon in general is sensitive to the magnesium/silicon ratio. If the (Fe+Mg)/Si ratio were unity, the moon would be all pyroxene with no calcium or aluminum. If it is less than unity, excess silica makes augite and calcium plagioclase in proportions such that the aluminum/calcium ratio resembles chondritic meteorites. An (Fe+Mg)/Si ratio of 0.8 needs twice as much calcium and aluminum to make its mineral suite than a ratio of 0.9, and so small changes in Mg/Si content can make large changes in Ca and Al content.

Deep Mysteries

The moon holds many mysteries and several were addressed at the conference. I. Garrick-Bethell and B. P. Weiss looked at the origins of lunar rock magnetism and the hypothesis that thermal cycling should have demagnetized any ancient lunar magnetism imposed on the rocks from an ancient lunar magnetic field. They presented t vs. T relations for Kamacite and showed that lunar rock magnetism is stable for billions of years and "almost certainly originated on the moon". Garrick-Bethell also looked at the fossil lunar tidal bulge and showed that the moment of inertia ratios are different than predicted for a tidally locked satellite.

J.J. Gillis-Davius, P.G. Lucey and B.R. Hawke did an analysis of Mare Moscoviense, a mare located in the thickest part of the lunar crust on the farside. With elevated iron oxide content, it is a window into the lunar interior. J.J. Hagerty et al also looked at the thorium abundances in the South Pole Aitken Basin and how they can help us understand the farside lunar mantle. B.R. Hawke et al also examined ancient volcanism of the Schiller-Schickard region for similar clues.

Perhaps one of the deepest mysteries was addressed in a paper at the Lunar and Planetary Science Conference by Y. Nakamura and C. Frohlich. Examining Apollo seismometer data, they found 12,500 seismic events. Twenty-eight of these are high-frequency teleseismic events, with distinguishable P and S waves (which normally are not distinguished on the moon) . These were originally thought to be caused by shallow moon quakes. However, 23 of the 28 occurred within hours of the time when the lunar nearside faced the Virgo cluster, that is, 12 hours Right Ascension (this means the moon would be at 0 hours Right Ascension as seen from Earth). Four events have farside origins; but for the 24 remaining, correlation with facing the Virgo cluster is good to 99.9% significance.

The largest of the high frequency teleseismic events was Richter magnitude 5, but most were smaller, of energy 1,000 to 100,000,000 joules. The authors first hypothesize that nuggets of strange quark matter, having a density of 100 trillion grams per cubic centimeter, might be responsible for these events, but eventually rule even this out because such high density objects would occur throughout the moon, not just shallowly below the crust.

Lunar Soil Simulants

At least two papers dealt with lunar soil simulants (earthen soil designed to mimic soil from the moon so that various analyses and tests of a destructive sort can be performed without using precious real lunar rock samples). M. M. Battler and colleagues at the University of New Brunswick developed a lunar anorthositic regolithic simulant using Earth-based Archean-age anorthosites. The simulants have small amounts of garnets and amphiboles, which are not found generally in lunar rocks. P. Carpenter et al looked at the development of a wide range of lunar soil simulants. K.S. Martirosyan and D. Luss explored ceramic synthesis from lunar soil simulants.

Epilog

The lunar papers at this conference showed a continued progress in understanding our sister world: answering some questions, revealing mysteries, almost calling us back to gather more data.

VISIBILITY OF THE ALUMINUM LINE IN THE SMART-1 IMPACT

By Francis G. Graham
Dept. Physics
Kent State University

Abstract

The aluminum line at 3961 Angstroms likely will not be visible during the SMART-1 impact on the lunar surface 2-3 Sept., 2006. The impact is too low a velocity to vaporize the entire spacecraft; any visibility will depend critically on the hydrazine and oxidizer ullage. It is estimated that about 2-10 kg of aluminum may be vaporized.

Introduction

The SMART-1 spacecraft, with approximately 200 kg of aluminum aboard, will impact the lunar surface at a glancing angle on 1-2 September, 2006 (Data from Foing, 2006). Would aluminum vapor be present in sufficient quantities to enable detection from Earth? The impact will be in lunar daylight and the emission of the aluminum line above the ambient continuum will be difficult to detect. There are four main aluminum lines: at 3082.53 Angstroms, 3092.7 Angstroms, 3944.0 Angstroms and the strongest, at twice the intensity of the 3082 line, at 3961.52 Angstroms. This latter line is also located in the flank of the wide "H" Fraunhofer line of Ca II in the reflected solar spectrum from the daylit moon. Hence, even a weak line might be detectable (Graham, 1996)

Limitations on Visibility

Unfortunately, the speed of the spacecraft will be below that needed for a hypervelocity impact. While the speed of sound in the upper heavily brecciated layer of the lunar surface is low, about 300 km./sec., this is due primarily to the circuitous route the acoustic waves must travel in the upper regolith. The solid material below the upper brecciated layer has a P-wave velocity of 4 km/sec., higher than the spacecraft velocity (Bott, 1982). Thus, the spacecraft will not have a hypervelocity impact, especially at a glancing angle. Instead, a portion of the aluminum will be friction-vaporized along a 2-3 km swath.

That portion is likely to be small. The amount of heat needed for total vaporization of all 200 kg of the aluminum is about 800 MJ, yet only about 400 MJ are available in the impact. With an efficiency of approximately 2% for friction vaporization, about 2 kg would actually get vaporized. The remainder of the aluminum, in solid and melt, would be strewn extensively over the lunar surface (Data from Reader, 2000).

Some hope lies with the hydrazine and oxidizer ullage that remains aboard the spacecraft on impact. Every 32 g of hydrazine, in an excess of oxidant, produces approximately 622 kJ at a combustion temperature of about 3400 K. Thus, 32 g of hydrazine in excess oxidant can vaporize about 6.7 kg η (η is the efficiency of the heating to the vaporization) of aluminum surrounding it, and this would occur at the point of impact. If $\eta = 10\%$, then about 700 grams of aluminum might be vaporized per mole of hydrazine. The amount of aluminum vapor formed on impact is thus dependent on the remaining hydrazine/oxidizer mixture. It is likely, however, that the efficiency will be even less, e.g. 1% or even 0.1%, and so the results can be scaled accordingly.

To sum up, we can expect, at maximum, on the order of $2 + 0.7\,M = m$ of aluminum vapor, where M is the number of surviving moles of hydrazine in excess oxidant.

Line Observability

As the impact fireball of aluminum vapor of mass m expands to radius r, it creates a volume density of $N_\lambda(4000m) / 3r^3$ and a column density $N_\lambda(1000m) / r^2 = d$. If the spectroscope slit length subtends r on the lunar surface, then this column density will determine the strength of the aluminum line. For a fireball less than the slit width which encompasses 2000 meters = r of the lunar surface, and the major length of the frictional vaporization trail from the glancing impact, $d \sim 9 \times 10^{19}$ for a 2000 gram vaporized mass.

The aluminum 3961 Angstrom line contains about 0.4 of the entire luminosity of the lines in the visible spectrum of aluminum. This is the population of atoms excited to the state.

In the visible range of the spectrum, for the aluminum line, therefore,

$$I = (0.4)gd(10^{-6}) \text{ rayleighs.}$$

where g is the photon scattering coefficient. We assume, $g \sim 0.5$

This is 6.3×10^{13} kR.

At about 4000 Angstroms, 1 kR = 39.5 pW cm^2/sec- steradian. (Barrington-Leigh, 2000). Since the impact swath will be cut and produce vapor in about 1 second, this is about 2500 watts- cm^2/str in the 3961 line for a 2 kg vaporized mass. This note may be generous in assumptions of the frictional vaporized mass. The author observed the impact site of Lunar Prospector with a spectrograph centered on the 3961 line, but the equipment used at the time was quite limited—a photographic spectrograph and a small college refractor. No aluminum vapor line was detected.

References:

Barrington-Leigh, Christopher (2000) Fast Photometric Imaging of High Altitude Flashes Above Thunderstorms Thesis.

Bott, Martin H.P. (1982) The Interior of the Earth Dodrecht: Elsevier p. 26-27

Foing, Bernard H. (2006) private communication.

Graham, Francis G. (2006) “A Search Strategy for Aluminum in the Lunar Atmosphere” LPSC XXVII p. 439-440

Reader, Joseph, and Corliss, Charles H. , (2000) “Line Spectra of the Elements” in Lide, David L. ed., Handbook of Physics and Chemistry 82nd ed. Boca Raton: CRC Press.

Aluminum Emission Line in the H line (simulated for higher impact velocity than expected)